

# Structure of Flame-Made Silica Nanoparticles by Ultra-Small-Angle X-ray Scattering

Hendrik K. Kammler, Gregory Beaucage,<sup>†</sup> Roger Mueller, and Sotiris E. Pratsinis\*

Particle Technology Laboratory, Department of Mechanical and Process Engineering, ETH Zurich, Sonneggstrasse 3, ML F25, CH-8092 Zurich, Switzerland

Received April 14, 2003. In Final Form: October 15, 2003

Ultra-small-angle X-ray scattering (USAXS) of agglomerated and nonagglomerated flame-made silica nanoparticles is investigated systematically for ubiquitous characterization of particle size and degree of agglomeration. Primary particle diameters determined from the USAXS particle volume to surface ratio were compared to those obtained from nitrogen adsorption (Brunauer–Emmett–Teller (BET)) measurements. Independent of the silica precursor state (vapor or liquid), production rate (5–1100 g/h), degree of agglomeration, or flame conditions (premixed, diffusion, or spray flame), there is excellent agreement between BET and USAXS for the average primary particle diameter. Furthermore, the USAXS data reveal the effect of the fuel and precursor flow rate for various vapor- and liquid-fed flame reactors on product primary particle diameter and agglomerate size.

## 1. Introduction

A number of ultra-fine metal and metal oxide particle products are made by aerosol processes, since they do not involve multiple steps and high liquid volumes associated with wet chemical processes. Such products are carbon black, fumed silica, zinc oxide, pigmentary titania, and filamentary nickel made at rates up to several tons per hour.<sup>1</sup> Hard agglomerates or simply agglomerates are particles connected by chemical bonds, while soft agglomerates (aggregates) are connected by physical (van der Waals, electrical, etc.) bonds following Kaye.<sup>2</sup> Agglomerates degrade the performance of paints, coatings, adhesives, and cosmetics, while they are sought in manufacture of lightguide preforms, reinforcing silicon rubber, catalysts, specialty elastomers, and chemical mechanical polishing.<sup>3</sup>

Previously, information about the degree of particle agglomeration, mass-fractal dimension,  $D_f$ , and agglomerate and primary particle size distributions was obtained most commonly from transmission electron microscopy (TEM) analysis. This is tedious and time-consuming when obtained manually or difficult to automatize through the occlusion of three-dimensional structures as typically 100–1000 particles need to be counted for reliable determination of the particle size distribution.<sup>4</sup> This is particularly challenging when nonspherical particles are encountered. As a result, there are very few reliable quantitative data on agglomerate characteristics (agglomerate size and mass-fractal dimension). For bulk characterization of the above products, the specific surface area obtained from nitrogen adsorption is often used from which an equivalent primary particle diameter is obtained. X-ray diffraction (XRD) determines the crystal size of the particles but cannot provide information about the size of the ag-

glomerates or the  $D_f$ . Light scattering of aqueous solutions of nanostructured powder has been combined with small-angle neutron scattering (SANS) to obtain from a combined scattering pattern the primary particle size (from SANS) and degree of agglomeration and fractal dimension (from light scattering).<sup>5</sup> Xing et al.<sup>6</sup> used multiangled light scattering to obtain in situ  $D_f$ , agglomerate radius, and volume fraction of flame-made alumina. The primary particle radius was obtained by thermophoretic sampling and microscopy that provided consistent results with light scattering with respect to the agglomerate properties. Cho and Choi<sup>7</sup> used 90° light scattering data with a structure factor<sup>8</sup> to obtain the number density and volume fraction of flame-made silica agglomerates that were assumed to be monodisperse. Furthermore, the mass-fractal dimension and the primary particle radius were obtained from thermophoretically collected samples and image analysis of the corresponding TEMs.

Ultra-small-angle X-ray scattering (USAXS), however, is capable of determining all characteristics of agglomerate and primary particles:  $D_f$ , radii of gyration (primary particles and agglomerates), and the powder volume to surface ratio ( $V/S$ ), using the unified fitting equation.<sup>9–11</sup> Limited data, however, are available for direct comparison between diameters obtained from (ultra-)small-angle X-ray scattering ((U)SAXS) and other techniques such as nitrogen adsorption (Brunauer–Emmett–Teller (BET)) or TEM: Fractal analysis of silica and titania nanoparticles was carried out for instance by Hyeon-Lee et al.,<sup>12</sup> where  $D_f$  values of 1.6–2.5 were measured for silica and titania agglomerates made in single and double diffusion flames.<sup>13</sup> Besides  $D_f$ , they reported the radius of gyration of primary ( $R_{g1}$ ) and agglomerate ( $R_{g2}$ ) particles, as well

\* Corresponding author. Tel: +41-(0)1-632-3180. Fax: -1595. E-mail: pratsinis@ptl.mavt.ethz.ch.

<sup>†</sup> Department of Materials Science and Engineering, University of Cincinnati, Cincinnati, OH 45221-0012.

(1) Pratsinis, S. E. *Prog. Energy Combust. Sci.* **1998**, *24*, 197.

(2) Kaye, B. H. *Characterization of powders and aerosols*; Wiley-VCH: Weinheim, 1999.

(3) Kammler, H. K.; Mädler, L.; Pratsinis, S. E. *Chem. Eng. Technol.* **2001**, *24*, 583.

(4) Tsantilis, S.; Kammler, H. K.; Pratsinis, S. E. *Chem. Eng. Sci.* **2002**, *57*, 2139.

(5) Hurd, A. J.; Schaefer, D. W.; Martin, J. E. *Phys. Rev. A* **1987**, *35*, 2361.

(6) Xing, Y.; Köylü, Ü. Ö.; Rosner, D. E. *Appl. Opt.* **1999**, *38*, 2686.

(7) Cho, J.; Choi, M. *J. Aerosol Sci.* **2000**, *31*, 1077.

(8) Oh, C.; Sorensen, C. M. *J. Aerosol Sci.* **1997**, *28*, 937.

(9) Beaucage, G. *J. Appl. Crystallogr.* **1995**, *28*, 717.

(10) Beaucage, G. *J. Appl. Crystallogr.* **1996**, *29*, 134.

(11) Beaucage, G.; Schaefer, D. W. *J. Non-Cryst. Solids* **1994**, *172*, 797.

(12) Hyeon-Lee, J.; Beaucage, G.; Pratsinis, S. E.; Vemury, S. *Langmuir* **1998**, *14*, 5751.

(13) Pratsinis, S. E.; Zhu, W.; Vemury, S. *Powder Technol.* **1996**, *86*, 87.

as the specific surface area and the number of primary particles per agglomerate. The USAXS silica primary particle diameter,  $d_{\text{sphere}} (=2(5/3)^{1/2}R_{\text{g}1})$ , was typically 2 times larger than the diameter obtained by BET, although for some titania powders they were in good agreement with each other. For Cab-O-Sil M-5 (Cabot), Hurd et al.<sup>5</sup> measured  $d_{\text{sphere}}$  to be 2.3 times larger than the  $d_{\text{BET}}$ . Similarly, Rieker et al.<sup>14</sup> found  $D_f = 1.7\text{--}2.1$  and  $d_{\text{sphere}}$  to be 2.7–3.1 times larger than the average primary particle diameter obtained from TEM for various commercial carbon black samples (Tokai Carbon Co., Ltd., Japan). Szekeres et al.<sup>15</sup> compared, however, the mean chord length,  $\bar{l}$ , and the chord lengths of the solid,  $l_1$ , and gas,  $l_2$ , phases using a nonparticulate model<sup>16</sup> to BET and other adsorption methods for Aerosil 200 (Degussa AG) and a microporous Stoeber silica powder. For the nonporous Aerosil 200, they reported good agreement between SAXS and BET primary particle diameters. Recently, Nakamura et al.<sup>17</sup> prepared very narrowly distributed gold nanoparticle solutions and compared particle diameters obtained from SAXS to TEM data. The primary particle diameter obtained from the slope of a Guinier plot was slightly larger than that obtained by TEM,  $d_{\text{TEM}}$ . After accounting for the effect of particle size distribution, the match between  $d_{\text{sphere}}$  and  $d_{\text{TEM}}$  was excellent.

Here a relatively large body of agglomerated and nonagglomerated silica data made in various flame reactors is analyzed systematically by USAXS, microscopy, and nitrogen adsorption. All agglomerate and primary particle characteristics are obtained by USAXS, while nitrogen adsorption and microscopy are only used to evaluate USAXS. The effects of process variables such as fuel and precursor flow rates of vapor- and liquid-fed flame aerosol reactors on the USAXS-determined silica primary particle diameter, agglomerate radius of gyration, and mass-fractal dimension are presented.

## 2. Experimental Section

Silica nanoparticles were produced in premixed and diffusion flame reactors.<sup>18</sup> For example, 17 g/h of these particles (Si-B 32) was made in a sustained premixed flame by flowing 2.9 L/min hexamethyldisiloxane (HMDSO)-laden nitrogen together with 4.7 L/min oxygen through the center tube of that reactor<sup>18</sup> and 1.4 L/min methane through its third tube. Likewise, silica particles were made in a diffusion flame microreactor<sup>19</sup> at 5 g/h and in a pilot-scale flame spray pyrolysis (FSP) unit<sup>20</sup> at 50–1100 g/h. Silica particles containing 0–1.5 wt % carbon<sup>21</sup> or 0–3.8 wt % titania<sup>22</sup> were produced at 125–700 g/h or 100–500 g/h, respectively, in a pilot-scale hydrogen–air diffusion flame reactor.

The product powder was collected on glass fiber filters (Whatman GF/A) that were placed typically 20 cm above the burner. In the pilot-scale units,<sup>20–22</sup> the powders were collected with baghouse filters. The BET specific surface area (SSA) of the powder was determined by nitrogen adsorption (Tristar, Micromeritics Instruments Corp.) from a five-point isotherm in the

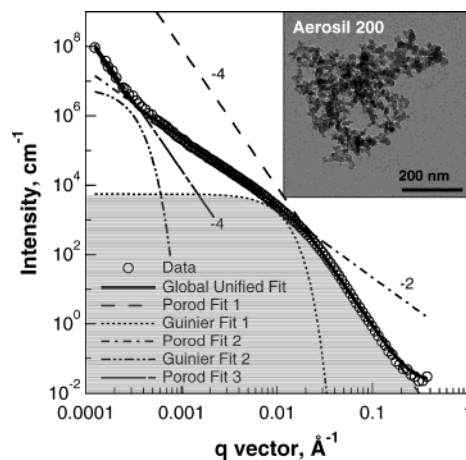


**Figure 1.** An USAXS pattern of agglomerated fumed silica (Aerosil 200, Degussa AG). The scattering data (circles) are well described by the global unified fit equation (solid line). Furthermore, three Porod regimes (dashed line, dashed–dotted line, and long–short-dashed line) are shown together with the Guinier regimes (dotted line and dashed–double-dotted line). The appearance of the second Porod (weak power-law) regime ( $0.0005 \text{ \AA}^{-1} < q < 0.01 \text{ \AA}^{-1}$ ) proves that these particles are agglomerated and mass fractal as shown by the TEM insert. The gray shaded area indicates the integral part for determination of  $d_{V/S}$ .

relative pressure range of 0.05–0.25.<sup>23,24</sup> The corresponding average primary particle diameter is calculated assuming spherical particles by  $d_{\text{BET}} = 6/(\rho_{\text{SiO}_2} \text{SSA})$ , using  $\rho_{\text{SiO}_2}$  of 2200 kg/m<sup>3</sup>. The TEM pictures are taken with a Zeiss electron microscope 912 Omega operated at 100 kV using a slow-scan CCD camera and the ProScan software. The TEM pictures of the filter powder are prepared by just dipping the TEM grid into the powder.

The USAXS pattern of the powders is measured under ambient pressure using a Bonse-Hart camera covering a  $q$  range of 0.0001–0.4  $\text{\AA}^{-1}$  (APS UNICAT Beamline ID-33) and 10 keV.<sup>25</sup> The employed photon beam was 0.4 mm high and 2 mm wide, and the momentum transfer vector,  $q$ , is calculated from  $q = 4\pi \sin(\theta/2)/\lambda$ , where  $\lambda$  is the wavelength of the employed irradiation and  $\theta$  is the scattering angle.<sup>26</sup> Powder samples of about 0.1 mm film thickness held between two strips of common transparent adhesive polymer (Scotch 810, 3M) were characterized by USAXS. These data were corrected for transmission and for background from the adhesive polymer, desmeared with UNICAT software (available on-line at [www.uni.aps.anl.gov](http://www.uni.aps.anl.gov)), and analyzed with software also available at UNICAT. The  $d_{V/S}$  is calculated from the USAXS particle volume to surface ratio as summarized in the next section, while the  $d_{\text{sphere}}$  is calculated as defined in the Introduction. Error bars represent the standard deviation of multiple reproduction (typically 2–3 times) of the USAXS or BET measurements of the respective powders. The error of the BET measurements is so small (<3%) that it is smaller than the symbol in the diagrams, although its absolute value depends on the adsorption molecules.<sup>27</sup>

## 3. Method of Analysis

Figure 1 shows the scattering pattern of a highly fractal and commercially available powder, Aerosil 200 (Degussa AG, SSA = 200 m<sup>2</sup>/g), while Figure 2 shows that of a

(14) Rieker, T. P.; Misono, S.; Ehrburger-Dolle, F. *Langmuir* **1999**, *15*, 914.

(15) Szekeres, M.; Toth, J.; Dekany, I. *Langmuir* **2002**, *18*, 2678.

(16) Porod, G. Small-angle X-ray scattering. In *Small-Angle X-ray Scattering*; Glatter, O., Kratky, O., Eds.; Academic Press: London, 1982; Part II, Chapter 2.

(17) Nakamura, K.; Kawabata, T.; Mori, Y. *Powder Technol.* **2003**, *131*, 120.

(18) Mueller, R.; Kammler, H. K.; Pratsinis, S. E.; Vital, A.; Beaucage, G.; Burtscher, P. *Powder Technol.*, in press (2004).

(19) Wegner, K.; Stark, W. J.; Pratsinis, S. E. *Mater. Lett.* **2002**, *55*, 318.

(20) Mueller, R.; Madler, L.; Pratsinis, S. E. *Chem. Eng. Sci.* **2003**, *58*, 1696.

(21) Kammler, H. K.; Mueller, R.; Senn, O.; Pratsinis, S. E. *AIChE J.* **2001**, *47*, 1533.

(22) Stark, W. J.; Kammler, H. K.; Strobel, R.; Gunther, D.; Baiker, A.; Pratsinis, S. E. *Ind. Eng. Chem. Res.* **2002**, *41*, 4921.

(23) Brunauer, S.; Emmett, P. H.; Teller, E. *J. Am. Chem. Soc.* **1938**, *60*, 309.

(24) Webb, P. A.; Orr, C. *Analytical methods in fine particle technology*; Micromeritics Instrument Corp.: Norcross, GA, 1997.

(25) Long, G. G.; Allen, A. J.; Ilavsky, J.; Jemian, P. R.; Zschack, P. The ultra-small-angle X-ray scattering instrument on UNICAT at the APS, SRI99. In *Eleventh U.S. National Synchrotron Radiation Instrumentation Conference*; American Institute of Physics: New York, 1999.

(26) Roe, R.-J. *Methods of X-ray and neutron scattering in polymer science*; Oxford University Press: New York, 2000.

(27) Ross, S. B.; Smith, D. M.; Hurd, A. J.; Schaefer, D. W. *Langmuir* **1988**, *4*, 977.

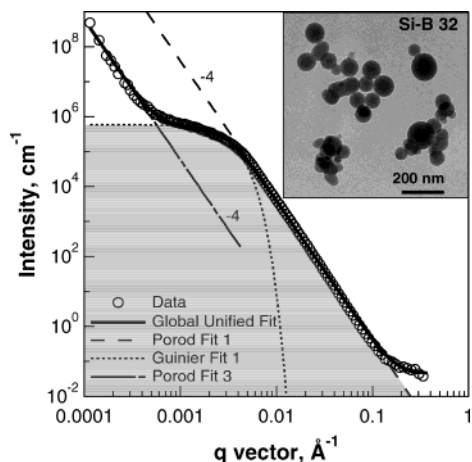


**Figure 2.** A USAXS plot of a nonagglomerated fumed silica (Si-B 32) made in a 17 g/h sustained premixed flame reactor (ref 18). The scattering data (circles) are well described by the global unified fit equation (solid line). Furthermore, Porod regimes (dashed line and long-short-dashed line) are shown together with the Guinier regime (dotted line). The lack of the Porod (weak power-law) regime at  $0.0005 \text{ \AA}^{-1} < q < 0.005 \text{ \AA}^{-1}$  indicates that the particles are nonagglomerated as shown by the TEM insert. The gray shaded area indicates the integral part for determination of  $d_{V,S}$ .

nonfractal  $\text{SiO}_2$  powder (Si-B 32,  $\text{SSA} = 32 \text{ m}^2/\text{g}$ ) made in the premixed flame reactor,<sup>18</sup> along with the corresponding TEM pictures. The scattering data (circles, Figures 1 and 2) are well described by the global unified fit analysis (solid lines, Figures 1 and 2).<sup>9,10</sup> Local Porod and Guinier scattering regimes are identified from this analysis as will be described here. Large scattering angles and thus high values of the momentum transfer vector,  $q$ , reflect small size,  $d$ , through Bragg's law,  $d = 2\pi/q$ .<sup>26</sup> At a high  $q$  ( $0.03\text{--}0.1 \text{ \AA}^{-1}$ ), the scattered intensity,  $I(q)$ , decays following a power-law (Porod's law)<sup>16,26</sup> (dashed line, Porod fit 1; Figures 1 and 2),

$$I(q) = Bq^{-4} \quad \text{where } B = 2\pi N(\Delta\rho)^2 S \quad (1)$$

Here,  $S$  is the average surface area of a particle and  $N$  is the number density of primary particles in the measured scattering volume, respectively, while  $\Delta\rho$  is the difference in electron density between the oxide nanoparticles and the background of primary particles.<sup>9–11</sup>

A power law of  $-4$  (dashed line, Porod fit 1; Figures 1 and 2) is observed for a smooth surface of the primary particles. This first power-law (Porod) regime is followed at lower  $q$  ( $\sim 0.01 \text{ \AA}^{-1}$ ) by a kneelike decay (Guinier) regime (dotted line, Guinier fit 1; Figures 1 and 2). This kneelike decay in intensity reflects the structural size of primary particles. In Figure 1, a second Guinier regime (dashed-double-dotted line, Guinier fit 2, at  $q \sim 0.0003 \text{ \AA}^{-1}$ ) is plotted that reflects the structural size of the hard agglomerates. This second Guinier regime is not present for the nonagglomerated powder in Figure 2. The scattering for these kneelike regimes follows Guinier's law,<sup>26,28</sup>

$$I(q) = G_i \exp\left\{-\frac{q^2 R_{gi}^2}{3}\right\} \quad \text{where } G_i = N_i(\Delta\rho)^2 V_i^2 \quad (2)$$

where  $N_i$  is the number density and  $V_i$  is the volume of a primary particle in the first ( $i=1$ ) Guinier regime (dotted line, Guinier fit 1; Figures 1 and 2) and the number density

and volume of an agglomerate in the second ( $i=2$ ) Guinier regime (dashed-double-dotted line, Guinier fit 2; Figure 1), respectively. Furthermore, from eq 2 the radius of gyration of the primary particles,  $R_{g1}$ , and the radius of gyration of the agglomerates,  $R_{g2}$ , can be derived.<sup>26</sup> The slope of the weak power-law decay between the two Guinier knees (dashed-dotted line, Porod fit 2; Figure 1) is directly related to the mass-fractal structure of the ramified agglomerates by<sup>12</sup>

$$I(q) = B_2 q^{-D_f} \quad (3)$$

where  $D_f$  is the mass-fractal dimension and  $B_2$  is a power-law prefactor,<sup>10</sup>

$$B_2 = \frac{G_2 D_f \Gamma \frac{D_f}{2}}{R_{g2}^{D_f}} \quad (4)$$

where  $G_2$  is a constant defined by eq 2 and  $\Gamma$  is the gamma function.<sup>10,12</sup>

In Figure 1, a third power-law (Porod) regime (eq 1) of slope  $-4$  (long-short-dashed line, Porod fit 3) is shown, which describes soft agglomerates (aggregates). This part of the scattering pattern, however, is not further investigated here, since a third Guinier regime is not observed. Similarly, this scattering signal is also observed in Figure 2 (long-short-dashed line, Porod fit 3) reflecting soft agglomerated primary particles consistent with the TEM insert.

Since these local scattering regimes overlap, as does the scattering from the adjacent particles, it is not appropriate to apply just the local scattering functions that neglect particle-particle scattering interactions. Therefore, in this work the global unified fit equation<sup>9–11</sup> is used (solid line in Figures 1 and 2), which describes the entire scattering pattern and is closely aligned to the local scattering laws described above. For Aerosil 200 (Figure 1), it yields<sup>12</sup>  $G_1 = 5250 \text{ cm}^{-1}$ ,  $R_{g1} = 18.8 \text{ nm}$ ,  $B_1 = 9 \times 10^{-5} \text{ cm}^{-1} \text{ \AA}^{-1}$ ,  $G_2 = 13.9 \times 10^6 \text{ cm}^{-1}$ ,  $R_{g2} = 1150 \text{ nm}$ ,  $D_f = 2.0$ , and  $B_2 = 0.25 \text{ cm}^{-1} \text{ \AA}^{-D_f}$ .

### 3.1. Primary Particle Diameter Determination.

Several choices to describe the primary particle diameter are possible such as  $d_{\text{sphere}}$  from  $R_{g1}$  as described above, or using various integrals of the scattering intensity versus  $q$ , leading to the cord length, and so forth.<sup>16</sup> In the present work, the primary particle diameter is derived from

$$d_{V,S} = \frac{6Q}{\pi B_1} \quad (5)$$

where the Porod invariant,  $Q$ , is the integral of the part of the scattering curve (indicated gray, Figures 1 and 2) associated with primary particles,

$$Q = \int_0^\infty q^2 I(q) dq = 2\pi^2 N(\Delta\rho)^2 V \quad (6)$$

Using Porod's law<sup>16</sup> (eq 1) together with eq 6, eq 5 becomes

$$d_{V,S} = \frac{6Q}{\pi B_1} = \frac{6 \times 2\pi^2 N(\Delta\rho)^2 V}{\pi \times 2\pi N(\Delta\rho)^2 S} = \frac{6V}{S} \quad (7)$$

This primary particle diameter reflects the ratio of the third to the second moment of the particle size distribution,  $d_{V,S} = M_{3,0}/M_{2,0}$ ,<sup>29</sup> the same moment as measured by nitrogen adsorption (BET).

(28) Guinier, A.; Fournet, G. *Small angle scattering of X-rays*; Wiley: New York, 1955.

(29) Hinds, W. C. *Aerosol Technology*; John Wiley and Sons: New York, 1999.

For one single particle, this  $V/S$  ratio is directly related to Porod's number-average chord length,  $\bar{l}$ , by<sup>16</sup>

$$\bar{l} = \frac{4V}{S} \quad (8)$$

The primary particle diameter obtained from the total particle volume to surface ratio is especially appealing since it can be compared directly to the average primary particle diameter obtained from BET,  $d_{\text{BET}} = 6/(\rho \text{ SSA})$ . The comparison can be made easily as the BET equivalent diameter is obtained from the mass to surface ratio of the particles, displaying exactly the same moment ratio as the  $d_{V/S}$  from USAXS.

#### 4. Results and Discussion

Three samples of Aerosil 200, of which one of them is shown in Figure 1, were analyzed, resulting in  $d_{V/S}$  of  $15.2 \pm 0.2$  nm, which is in excellent agreement with  $d_{\text{BET}}$  of  $14 \pm 0.4$  nm. The  $D_f$  of this powder is  $2.2 \pm 0.2$ , the  $R_{g1}$  is  $18.7 \pm 0.4$  nm, and  $R_{g2}$  is  $1200 \pm 80$  nm. From the radius of gyration of the primary particles,  $R_{g1}$ , a corresponding diameter  $d_{\text{sphere}} = 2(5/3)^{1/2}R_{g1} = 48.3$  nm can be calculated assuming monodisperse spherical particles,<sup>12</sup> which is here 3.4 times the  $d_{\text{BET}}$ . A similar difference of  $d_{\text{sphere}}$  and  $d_{\text{BET}}$  was found also for carbon black by Rieker et al.<sup>14</sup> and for  $\text{SiO}_2$  by Hurd et al.<sup>5</sup> and Hyeon-Lee et al.<sup>12</sup> The  $R_{g1}$  is obtained from high moments of the particle size distribution so it becomes apparent why a consistent ratio of moments is necessary for a valid comparison. The Aerosil 200 is clearly agglomerated in agreement with the manufacturer's specifications although this was reported as nonfractal by Szekeres et al.<sup>15</sup> It seems that their range of the momentum transfer vector  $q$  was not large enough to detect the mass-fractal region.

For nonagglomerated particles (Figure 2), the mass-fractal regime (second Porod regime, dashed-dotted line in Figure 1 for agglomerated particles) vanishes as a result of the loss of correlation between primary particles.<sup>30</sup> The global unified equation (solid line, Figure 2)<sup>9,10</sup> describes well the scattering data (circles) with one Guinier (dotted line, Guinier fit 1; Figure 2) and two Porod (dashed line, Porod fit 1 and long-short-dashed, Porod fit 3; Figure 2) regimes. This is observed also for titania nanoparticles<sup>12,13</sup> made in diffusion flames. Thus, SAXS data can be used also to decipher if nanostructured powders are agglomerated (fractal) or nonagglomerated (nonfractal) as has been demonstrated for oxides<sup>12</sup> and carbon blacks.<sup>30,31</sup>

**4.1. Comparison of  $d_{\text{BET}}$  and  $d_{V/S}$ .** Figures 3 and 4 compare the average primary particle diameters  $d_{V/S}$  and  $d_{\text{BET}}$  for various agglomerated (54 samples in Figure 3) and nonagglomerated (21 samples in Figure 4) silicas. Figure 3 shows also silica particles containing small amounts of carbon (0–1.5 wt %)<sup>21</sup> (diamonds) or  $\text{TiO}_2$  (0–3.8 wt %)<sup>22</sup> (circles). Furthermore, commercial silicas (Aerosil 200 (dark triangle) and Aerosil 380 (gray triangle), Degussa AG) are shown. Figure 3 shows also pure silica powders made in premixed (filled squares) and diffusion (open squares) flames.<sup>18</sup> Pure silica made by FSP at 50–300 g/h<sup>20</sup> (open triangles) is shown as well. The correlation coefficient,<sup>32</sup>  $r$ , between  $d_{\text{BET}}$  and  $d_{V/S}$  is 0.92, indicating a rather good agreement between the two measurements.

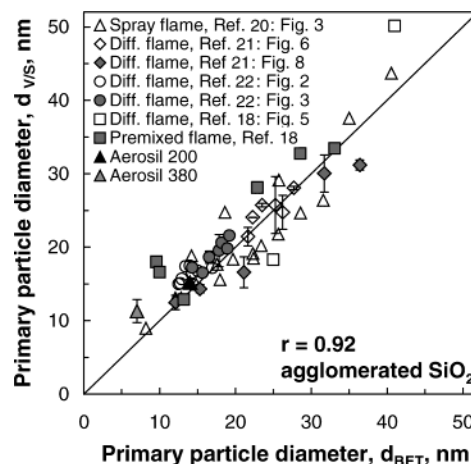


**Figure 3.** Comparison of  $d_{V/S}$  and  $d_{\text{BET}}$  for agglomerated silica powders made in our vapor- or liquid-fed flame aerosol reactors (refs 18 and 20–22) and those of commercially available powders (Aerosil 200 and Aerosil 380, Degussa AG).

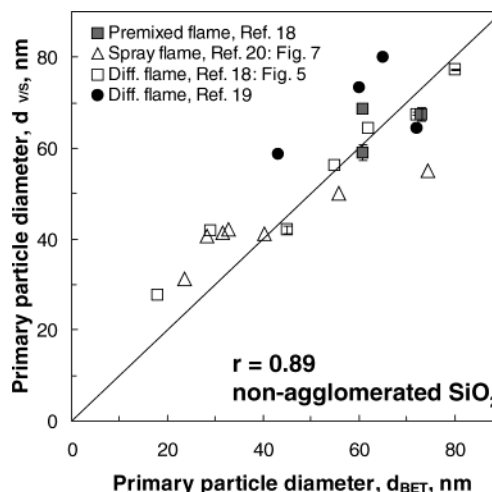


**Figure 4.** Comparison of  $d_{V/S}$  and  $d_{\text{BET}}$  for various nonagglomerated silica powders made in our vapor-fed (refs 18 and 19) and liquid-fed (ref 20) flame aerosol reactors.

The average value comparing the two techniques ( $d_{V/S}/d_{\text{BET}}$ ) is  $1.09 \pm 0.22$ .

Figure 4 shows the comparison of  $d_{\text{BET}}$  and  $d_{V/S}$  for nonagglomerated fumed silica powders. They were made in sustained premixed flames (filled squares) and diffusion flames (open squares).<sup>18</sup> Furthermore, pure silica made in a diffusion flame microreactor<sup>19</sup> by Wegner et al. (dark circles) is shown together with flame-spray-made silica at production rates of 300–1100 g/h (triangles).<sup>20</sup> The correlation coefficient,<sup>32</sup>  $r$ , is 0.89, while the average value comparing the two techniques ( $d_{V/S}/d_{\text{BET}}$ ) is  $1.09 \pm 0.21$  (Figure 4) which is comparable to that obtained for the agglomerated powders (Figure 3). So, the degree of agglomeration does not seem to affect the correlation between the  $d_{V/S}$  and  $d_{\text{BET}}$  (Figures 3 and 4).

The error in the USAXS measurement is calculated from the propagated counting error in the scattering data that is generally very low. The USAXS measurement is normalized internally by the Porod invariant  $Q$ . The USAXS analysis presented here relies on the particle surface being smooth and sharp, an assumption of Porod's law (eq 1). This assumption can be verified through observation of a scattering regime with a slope of  $-4$  in the log–log plots. This is clearly a good assumption for the data shown in Figures 1 and 2 (dashed line, Porod fit 1). The USAXS also relies on the accuracy of the global

(30) Rieker, T. P.; Hindermann-Bischoff, M.; Ehrburger-Dolle, F. *Langmuir* **2000**, *16*, 5588.

(31) Weth, M.; Mathias, J.; Emmerling, A.; Kuhn, J.; Fricke, J. *J. Porous Mater.* **2001**, *8*, 319.

(32) Papula, L. *Mathematik für Ingenieure und Naturwissenschaftler*, Band 3; Vieweg Verlag: Braunschweig, 2001; or Microsoft Excel math. function "correl".

unified fit in separating the primary particle structure from other structures present in the scattering curve, that is, the mass-fractal structured agglomerates and the structure of soft agglomerates. It is difficult to quantify the error involved in this separation. However, it is expected that this error would be higher for mass-fractal samples. Since there is no indication of a difference between the results for mass-fractal (agglomerated) and non-mass-fractal (nonagglomerated) samples shown in Figures 3 and 4, the global unified fit performs well in this regard. In general, even though both techniques rely on the indicated assumptions, the agreement between  $d_{V/S}$  derived from the Porod invariant (eq 6) and BET is quite good.

**4.2. Primary and Agglomerate Size and Mass-Fractal Dimension. 4.2.1. Effect of Hydrogen and HMDSO Flow Rate (in Turbulent Diffusion Flames).** The USAXS can be used also for exploring the effect of process parameters such as the hydrogen flow rate on the characteristics of agglomerates made at various conditions, for example, at  $\text{SiO}_2$  production rates of 300 g/h using a constant air flow rate of 120 L/min.<sup>21</sup> Figure 5a shows good agreement between the average primary particle diameter from nitrogen adsorption reported by Kammler et al.<sup>21</sup> and the present USAXS measurements. Both techniques show a smooth increase of the primary particle diameter from 22 to 28 nm with increasing hydrogen flow rate that can be directly related to an increase in flame temperature.<sup>21</sup> The mass-fractal dimension of these powders is between 1.6 and 2.1 and does not show a significant trend within experimental error (Figure 5b). This range of  $D_f$  is typical for flame-aerosol-made particles.<sup>5,33</sup> The agglomerate size ( $=2R_{g2}$ ) is around 5000 nm, and no significant effect of the hydrogen flow rate (Figure 5b) was found. Apparently, increasing hydrogen flow rate increases the process temperature and particle sintering rate that increases the primary particle size but does not affect the agglomerate size. Probably the small increase of the primary particle size comes from the increasing neck size between particles rather than collapsing them entirely to form bigger primary particles. As a result, the size of the agglomerates remains rather intact.

Figure 6a shows the effect of  $\text{SiO}_2$  production rate on the average primary particle diameter at hydrogen and air flow rates of 12.2 and 103 L/min, respectively.<sup>21</sup> When the production rate is increased from 125 to 700 g/h, the average primary particle size increases from 12 to 36 nm as determined by both BET and USAXS (Figure 6a), since the  $\text{SiO}_2$  concentration increases which leads to more collisions between the particles. For larger powder production rates of  $\geq 300$  g/h, the  $d_{\text{BET}}$  is larger than the  $d_{V/S}$ . A pronounced development of sintering necks (see TEM image inserted in Figure 6a) can explain the higher  $d_{\text{BET}}$  compared to  $d_{V/S}$  (Figure 6a) since less surface area is available. More fuel (as the HMDSO acts as fuel itself) increases the flame temperature and the flame height; thus, the particle growth rate is enhanced by the higher temperatures and the prolonged particle residence time at high temperatures. Both lead to the formation of larger primary particles<sup>21</sup> and more pronounced sintering necks that could explain the larger  $d_{\text{BET}}$  compared to  $d_{V/S}$  at higher production rates (Figure 6a). The TEM picture of the product particles shows relatively uniform primary particles in the agglomerates. At the highest production rates (especially at 700 g/h), agglomerates with broader size ranges are formed consisting of primary particles still

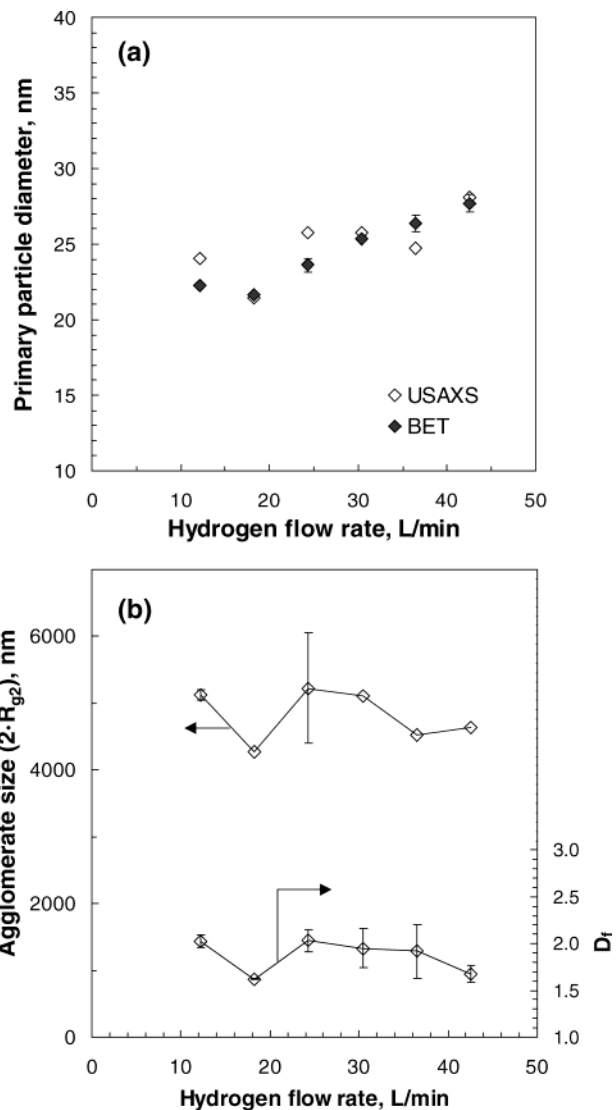


**Figure 5.** The effect of hydrogen flow rate on (a) the average primary particle diameter by USAXS and BET and (b) the agglomerate size ( $2R_{g2}$ ) and the mass-fractal dimension,  $D_f$  (USAXS), of vapor-fed flame-made silica powders. Increasing the hydrogen flow rate increases flame temperature that increases primary particle size but leaves intact the agglomerate size and the  $D_f$ .

relatively narrowly distributed within one agglomerate. The primary particle size varies, however, between different agglomerates (see overlapping agglomerates in the TEM of Figure 6a at 700 g/h). The latter can be attributed to variations of residence time and temperature history. It may be reflected also in a relatively low mass-fractal dimension of  $D_f = 1.5\text{--}1.6$  compared to the other agglomerated flame-made particles of Figure 1, 3, and 5, which typically have mass-fractal dimensions between 1.8 and 2.2, in agreement with earlier works.<sup>5,12,33</sup>

Increasing the silica concentration increased drastically the primary particle diameter (Figure 6a) but to a lesser extent the agglomerate size, from 1400 to 1700 nm (Figure 6b). If the agglomerate size had increased without changing the primary particle size, one would have expected to see an increase of agglomerate size by a factor of  $(700/125)^{(1/D_f)} = 2.4$  instead of an increase of  $1700 \text{ nm}/1400 \text{ nm} = 1.2$  observed here for increasing the production rate from 125 to 700 g/h.<sup>33</sup> However, the drastic increase of the primary particle diameter prevented that growth of agglomerate size. Furthermore, the agglomerates

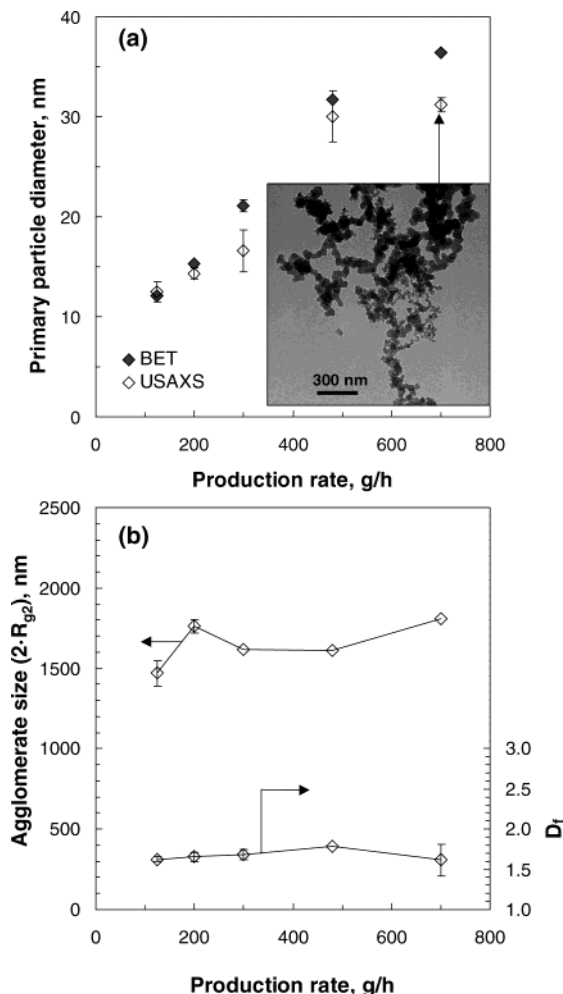


**Figure 6.** The effect of silica production rate on (a) the average primary particle diameter by USAXS and BET and (b) the agglomerate size ( $2R_{g2}$ ) and the mass-fractal dimension,  $D_f$  (USAXS), of vapor-fed flame-made silica powders. Increasing the silica production rate increases silica concentration and flame temperature that both drastically increase primary particle size but leave intact the agglomerate size and the  $D_f$ .

formed here are smaller than those obtained for the particles made at higher air flow rates (Figure 5b). From this comparison, it may be concluded that increasing turbulence and/or decreasing flame temperatures increase agglomerate size.

**4.2.2. Effect of Production Rate during FSP Synthesis of Silica.** Figure 7 shows the effect of production rate on the average primary particle size (Figure 7a), the agglomerate size ( $2R_{g2}$ ), and the mass-fractal dimension  $D_f$  (Figure 7b) during synthesis of silica by FSP using an air dispersion flow rate of 12.5 L/min.<sup>20</sup> Increasing the production rate increases the average primary particle diameter significantly from 8 to 27 nm, which can also be seen in the corresponding TEM pictures (inserts of Figure 7a). The increase of primary particle size can be attributed to the increase in  $\text{SiO}_2$  concentration and in flame temperature by the increased enthalpy and particle residence time in the hot flame region since more fuel increases the flame height and accelerates particle growth by coagulation and sintering.<sup>20</sup> The  $d_{\text{BET}}$  and the  $d_{\text{USAXS}}$  are in agreement for production rates of 50–150 g/h, while above that the  $d_{\text{USAXS}}$  is slightly smaller than the  $d_{\text{BET}}$  as was also observed for the vapor flame (Figure 6a). The average primary particle diameter of the FSP-made powder is higher than that made at the same production rate in the vapor flame, and this could be explained by the higher

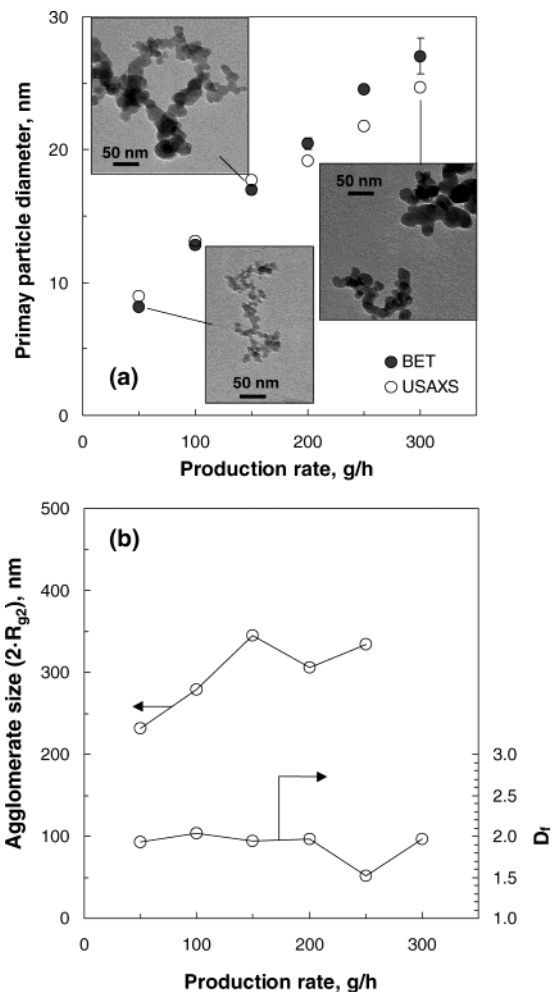


**Figure 7.** The effect of silica production rate on (a) the average primary particle diameter by USAXS and BET and (b) the agglomerate size ( $2R_{g2}$ ) and the mass-fractal dimension,  $D_f$  (USAXS), of silica powders made by FSP. Increasing the production rate increases both primary and agglomerate size at production rates of  $\leq 150$  g/h. Above that, primary particle diameter continues to increase but the agglomerate size somehow levels off as the agglomerate undergoes consolidation as shown by the TEM inserts. The  $D_f$  is not affected by the production rate.

temperature of the spray flame as shown later on. The mass-fractal dimension of the FSP-made powders is typically between  $D_f = 1.9$  and 2.0 (Figure 7b) and is in the range of values for vapor-fed flame-made oxide particles.<sup>5,12,33</sup>

The agglomerate size of FSP-made silica first increases at low production rates and then is almost constant around 330 nm for the higher ones (Figure 7b). The higher flame temperatures and prolonged particle residence time arising from the increasing flame height accelerate sintering and reduce agglomerate size. However, with increasing production rate the silica concentration increases also, so bigger particles are formed by coagulation that increase the agglomerate size. This is most pronounced at low production rates ( $\leq 150$  g/h), where a 3-fold increase in concentration increases the agglomerate size from 230 nm (at 50 g/h) to 350 nm (at 150 g/h). For  $D_f = 2$  (Figure 7b), the increase in agglomerate particle diameter ( $350 \text{ nm}/230 \text{ nm} = 1.5$ ) is consistent with an increase by a factor of  $(150/50)^{(1/D_f)} = 1.7$  for coagulation only. At higher production rates, the agglomerate size does not change as much since significant consolidation seems to take place on the agglomerate (see insert of Figure

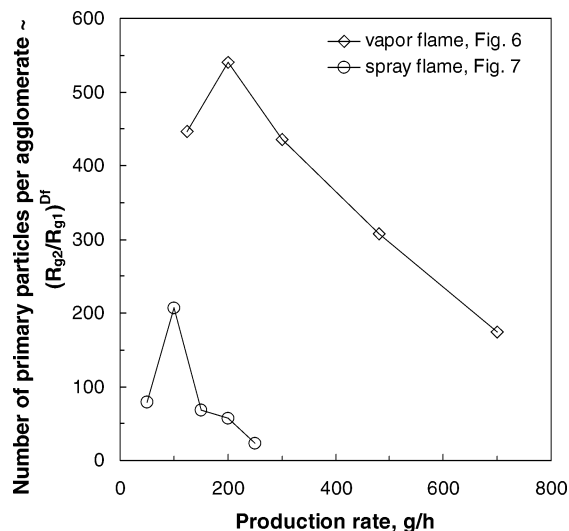


**Figure 8.** The number of primary particles per agglomerate  $N_p \sim (R_{g2}/R_{g1})^{D_f}$  as determined by USAXS as a function of the silica production rate for the data presented in Figures 6 and 7. At high production rates ( $> 150$  g/h), the  $N_p$  decreases with increasing production rate in the vapor-fed (diamonds) and liquid-fed (spray) flames as primary particles sinter by experiencing prolonged residence times at high temperatures.

7a at 300 g/h) though the fractal structure does not change (Figure 7b). In contrast, for the vapor-fed flames at production rates of the same order of magnitude the agglomerate size was increased slightly with production rate (Figure 6b).

The consolidation is reflected especially in the number of primary particles in an agglomerate,  $N_p$ .<sup>33</sup>

$$N_p \sim \left( \frac{R_{g2}}{R_{g1}} \right)^{D_f} \quad (9)$$

This proportionality is plotted versus the particle production rate in Figure 8 using the data presented partly already in Figures 6 and 7. With increasing production rate, the number of primary particles per agglomerate is decreased since  $R_{g1}$  increases faster than  $R_{g2}$  for both processes. At high production rates ( $> 150$  g/h), the  $N_p$  decreases with increasing production rate in the vapor- and liquid-fed (spray) flames as primary particles sinter by experiencing prolonged residence times at high temperatures.

However, agglomerate sizes of the FSP powders are smaller than the ones made in the vapor flames (Figure 6b) and the agglomerates consist of fewer primary particles per agglomerate (Figure 8). This is a result of the shorter residence time and the higher flame temperature in the FSP (adiabatic flame temperature increases from 3970 K

at 50 g/h to 4750 K at 150 g/h and to 5050 K at 300 g/h) than in the vapor-fed flames (adiabatic flame temperature increases from 1665 K at 125 g/h to 2375 K at 300 g/h to 2560 K at 700 g/h). This is reflected also by the more compact structure of the agglomerate made by FSP having a slightly higher mass-fractal dimension (Figure 7b) than the corresponding vapor-flame-made particles (Figure 6b) and fewer primary particles per agglomerate (Figure 8).

## 5. Concluding Remarks

The USAXS can distinguish between agglomerated and nonagglomerated flame-made silica particles. A detailed quantitative comparison was carried out between the average primary particle diameters from nitrogen adsorption (BET) analysis and from the Porod invariant for the primary particles of USAXS measurements. The excellent agreement between these two techniques was independent of the powder precursor state fed to the flame (vapor or liquid), the production rate (5–1100 g/h), or the flame conditions (premixed or diffusion flame or flame spray). The USAXS data showed that the agglomerate size of vapor-fed flames did not change significantly with increasing powder production rate especially with increasing hydrogen fuel flow rate. Nevertheless, the agglomerate size increased more dramatically with production rate for liquid-fed flame aerosol reactors until it reached a size where significant rearrangement and consolidation took place, as liquid-fed flames are hotter than vapor-fed ones. Smaller agglomerates were formed in liquid-fed than in vapor-fed flames as shorter residence time and higher flame temperature were employed in the former than in the latter ones. The mass-fractal dimension of agglomerated  $\text{SiO}_2$  particles was rather invariant with process parameters and ranged from 1.6 to 2.2 in vapor-fed flames and from 1.9 to 2.0 in liquid-fed flame aerosol reactors.

**Acknowledgment.** The UNICAT facility at the Advanced Photon Source (APS) is supported by the University of Illinois at Urbana–Champaign, Materials Research Laboratory (U.S. DOE, the State of Illinois-IBHE-HECA, and the NSF), the Oak Ridge National Laboratory (U.S. DOE under contract with UT-Battelle LLC), the National Institute of Standards and Technology (U.S. Department of Commerce), and UOP LLC. The APS is supported by the U.S. DOE, Basic Energy Sciences, Office of Science, under Contract No. W-31-109-ENG-38. We further acknowledge the financial support by the NSF (CTS-9986656 and CTS-0070214 to G. Beaucage) and the Swiss National Science Foundation (2100-063632.00/1 and 200021-101901/1). We thank Dr. Karsten Wegner for providing various powder samples and Dr. Martin Müller (both ETH Zurich) for providing the TEM facilities.

LA030155V